ACS APPLIED MATERIALS & INTERFACES

Research Article

www.acsami.org

Layer-by-Layer (LBL) Self-Assembled Biohybrid Nanomaterials for Efficient Antibacterial Applications

Yuanhao Wu,[†] Yubo Long,[†] Qing-Lan Li,[‡] Shuying Han,[§] Jianbiao Ma,[†] Ying-Wei Yang,*[,‡] and Hui Gao*[,†]

[†]School of Chemistry and Chemical Engineering, School of Material Science and Engineering, Tianjin Key Laboratory of Organic Solar Cells and Photochemical Conversion, Tianjin University of Technology, Tianjin 300384, China

[‡]State Key Laboratory of Inorganic Synthesis and Preparative Chemistry, College of Chemistry, International Joint Research Laboratory of Nano-Micro Architecture Chemistry (NMAC), Jilin University, 2699 Qianjin Street, Changchun 130012, People's Republic of China

[§]Department of Pharmacology, School of Basic Medical Sciences, North China University of Science and Technology, Tangshan 063000, People's Republic of China

Supporting Information

ABSTRACT: Although antibiotics have been widely used in clinical applications to treat pathogenic infections at present, the problem of drug-resistance associated with abuse of antibiotics is becoming a potential threat to human beings. We report a biohybrid nanomaterial consisting of antibiotics, enzyme, polymers, hyaluronic acid (HA), and mesoporous silica nanoparticles (MSNs), which exhibits efficient *in vitro* and *in vivo* antibacterial activity with good biocompatibility and negligible hemolytic side effect. Herein, biocompatible layer-by-layer (LBL) coated MSNs are designed and crafted to release encapsulated antibiotics, e.g., amoxicillin (AMO), upon triggering with hyaluronidase, produced by various pathogenic *Staphylococcus aureus* (*S. aureus*). The LBL coating process comprises lysozyme (Lys), HA, and 1,2-ethanediamine (EDA)-modified polyglycerol methacrylate (PGMA). The Lys and cationic polymers provided multivalent interactions between MSN-Lys-HA-PGMA and bacterial membrane and accordingly immobilized the nanoparticles to facilitate the synergistic effect of these antibacterial agents. Loading process was characterized by dynamic light scattering (DLS), transmission electron microscopy (TEM), thermogravimetric analysis (TGA), and X-ray diffraction spectroscopy (XRD). The minimal inhibition concentration (MIC) of MSN-Lys-HA-PGMA treated to antibiotic resistant bacteria is much lower than that of isodose Lys and AMO. Especially, MSN-Lys-HA-PGMA exhibited good inhibition for pathogens in bacteria-infected wounds *in vivo*. Therefore, this type of new biohybrid nanomaterials showed great potential as novel antibacterial agents.

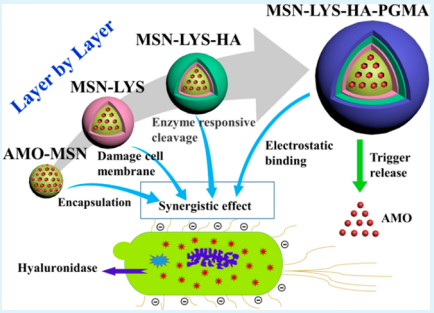

KEYWORDS: *antibacterial materials, layer-by-layer self-assembly, MSN, synergistic effects, lysozyme, enzyme response, cationic polymers, biohybrid nanoparticles*

INTRODUCTION

Individuals have been benefiting from the marketing of antibiotics that have been widely used in clinical applications. However, overuse of antibiotics has arguably led to a widespread outbreak of an infectious disease of drug-resistant microbes,[1,2] while limiting the use of antibiotics will probably sacrifice patient treatments.[3,4] Thus, it is urgent to develop novel antibacterial agents. During the past decades, cationic polymers,[5−18] polypeptides,[19−22] and inorganic nanoparticles[23−26] have been reported to show promising antibacterial activities.

In recent years, antibacterial polymers have been designed and synthesized as successful alternatives to traditional antibiotics.[15−18] Among them, cationic polymers have a great number of positive charges and cytoplasmic membrane-damaging activity toward negatively charged phospholipids of bacterial cell membrane, showing high selectivity for bacteria over mammalian cells and effective antibacterial activity against fungi, pathogens, and viruses.[27−31]

Lysozyme (Lys) is primarily bacteriolytic toward Gram-type positive strains,[32,33] caused by the fact that Lys has a relatively weak antimicrobial activity for Gram-negative bacteria, compared with Gram-positive bacteria, because of the protection of lipopolysaccharide layer surrounding their outmost membrane. Because of the weak antibacterial activity of cationic polymers, Lys can not only damage the wall/membrane of *E. coli* but also lead to the death of *E. coli*, which may facilitate the multivalent effects of polymers and antibiotics.

Received: May 14, 2015
Accepted: July 20, 2015
Published: July 20, 2015

© 2015 American Chemical Society

DOI: 10.1021/acsami.5b04216
ACS Appl. Mater. Interfaces 2015, 7, 17255−17263

Hyaluronic acid (HA) also shows bacteriostatic effects,[34] as well as antimicrobial and antiviral effects.[35,36] In addition, HA also contributes to the wound healing processes by promoting early inflammation.[37−39] The cationic polymer (e.g., 1,2-ethanediamine (EDA)-modified polyglycerol methacrylate (PGMA)) used in this study does not show specific target toward the bacteria, while HA could be used as an negative layer, and work as an enzyme hyaluronidase-responsive valve for antibacterial cargo, because the bacteria secreted enzyme hyaluronidase, being capable of enzymolysising hyaluronic acid (HA).[40−42]

Recently, mesoporous silica nanoparticles (MSNs) have been widely applied, because of their well-defined pore geometry, tunable pore size, large pore volume, and chemical stability.[43−48] Variety of capping agents, such as organic and inorganic molecules,[49−52] supramolecular assemblies,[53] and polymers,[54] have been employed to construct MSN-based cargo.[55−59] Lys-coated MSNs can act as efficient antibacterial agents with good biocompatibility.[18] However, the antibacterial ability of Lys alone was rather weak and the pores of MSNs were not fully utilized. Thus, we propose, for the first time, to load amoxicillin (AMO) as a model drug with effective and broad-spectrum antibacterial activities in the pores of MSN, after AMO molecules being loaded into the MSN, Lys, HA, and PGMA derivatives are allowed to be coated on MSN surfaces via layer-by-layer (LBL) self-assembly method (Scheme 1). These biohybrid nanoparticles are expected to exhibit good synergistic antimicrobial effect and antibacterial efficiency.

Scheme 1. Schematic Representation of the Layer-by-Layer (LBL) Process of MSN-Lys-HA-PGMA and the Possible Antimicrobial Mechanism for Each Layer

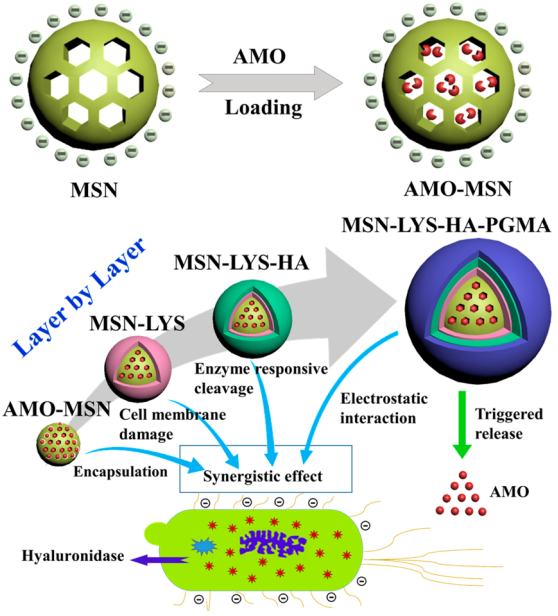

EXPERIMENTAL SECTION

Materials. Lys, HA and AMO were purchased from Sigma−Aldrich (Shanghai, China). Cetyltrimethylammonium bromide (CTAB) and 3-(triethoxysilyl)propyl isocyanate (ICPTES) were purchased from Aladdin Co. Ltd. (Shanghai, China). 1,2-Ethanediamine (EDA), tetraethyl orthosilicate (TEOS), and all other reagents were purchased from Tianjin Chemical Reagent Co. Ltd. (Tianjin, China). Cell Counting Kit-8 (CCK-8) was obtained from Dojindo (Beijing, China), and all other biological agents and consumable items were from Lifaxiang Reagent Co. Ltd. (Tianjin, China). PGMA was synthesized by atom transfer radical polymerization (ATRP). EDA-PGMA was synthesized according to our previously reported procedures.[7,8]

Preparation of MSN-COOH. MSNs were synthesized according to previous methods.[43−45] CTAB (1.0 g) was dissolved in deionized H_2O (240 mL) and then aqueous NaOH solution (3.5 mL, 2 M) was added. The mixture was heated to 80 °C under stirring for 30 min to get pellucid solution. Then, TEOS (5.0 mL) and ICPTES (0.6 mL) were added via injection sequentially and rapidly. Following the injection, a white precipitate was formed during 15 min of stirring at 1500 rpm. The reaction mixture was heated at 80 °C for another 2 h, and the products were isolated by hot filtration and washed with an extensive amount of H_2O and methanol (MeOH). To remove the templating surfactants from the mesopores, the as-synthesized silica nanoparticles (1.0 g) was suspended in acidic MeOH (MeOH: 100 mL; conc. HCl: 1.0 mL), and then refluxed for 6 h. The solvent extracted nanoparticles were collected by centrifugation, washed with MeOH, and dried under vacuum to give MSN-COOH. We will use MSN to represent carboxylated MSNs in the following text.

Loading of AMO into MSN. The MSN samples were dispersed into the aqueous solution of AMO (3 mg mL^{-1}) and stirred for 2 days at room temperature. The mixture was shaken for 10 min at 200 rpm and at room temperature. The free AMO was removed by centrifugation. The precipitate was then gently washed with water in triplicate until no free AMO was detected in the supernatant. The obtained precipitation was named as AMO-MSN. The amount of AMO was determined by measuring the UV absorbance of AMO in the supernatant at 385 nm. In order to determine the amounts of the components of AMO, we presented the concept of loading capacity:

$$\text{loading capacity (\%w/w)} = \frac{\text{mass of loaded guest}}{\text{mass of nanoparticles}} \times 100$$

Layer-by-Layer Self-Assembly. The concentration of the positively charged Lys solutions was fixed as 1 mg mL^{-1} in PBS solution (0.02 M, pH 6.2). First, AMO-MSN was immersed into Lys solution (50 mL) for 20 min, followed by rinsing with Mili-Q water for 2 min, to obtain MSN-Lys. The MSN-Lys then was incubated overnight with 0.2 mg mL^{-1} of HA at 15 °C, followed by rinsing to produce MSN-Lys-HA nanoparticles. The nanoparticles and EDA-PGMA (20 mg) then were added into PBS (pH 6.2, 50 mL) and stirred for 30 min, followed by centrifugation/dispersion twice with Mili-Q water for 1 min and then lyophilized, to obtain the final MSN-Lys-HA-PGMA. The MSN-Lys, MSN-Lys-HA, and MSN-Lys-HA-PGMA were all loaded with AMO cargo.

Transmission Electron Microscopy (TEM) and Field-Emission Scanning Electron Microscopy (SEM). The samples were dispersed in PBS (pH 7.4), deposited on carbon-coated copper grids, and dried in air. TEM experiments were carried out on a Model JEM-200CX microscope (JEOL, Japan). SEM was conducted at an accelerate voltage of 300 kV using a Model JSM-6700F microscope (JEOL, Japan). The samples (0.5 mg mL^{-1}) were dispersed ultrasonically in PBS and dried in air. Gold coating of nanoparticles for imaging was carried out by sputtering for 90 s.

***In Vivo* Antibacterial Effect of MSN-Lys-HA-PGMA.** To evaluate the *in vivo* antibacterial effect of MSN-Lys-HA-PGMA, the AMO-resistant *S. aureus* infection model was built. Hair from the back of each mouse was shaved with a fine-tooth electric clipper and the exposed skin was burnished with a scraper to ooze blood. The size of the wound was consistently 1 cm × 1 cm. Mice were anaesthetized when the trauma was induced. Each wound was inoculated with 50 μL of the indicated bacteria suspended in the LB broth (the concentration was ~5×10^6 CFU mL^{-1}). These samples were extracted with 100 μL and coated on a Petri dish after 16 h. Finally, we count the colony of bacteria as the ultimate content after 24 h of incubation. For each study, it included a uninfected group that did not receive any treatment, one group that received singly transdermal drug delivery with AMO & Lys, and another group that received transdermal MSN-Lys-HA-PGMA at the same dosages as the singly treated groups. For

DOI: 10.1021/acsami.5b04216
ACS Appl. Mater. Interfaces 2015, 7, 17255−17263

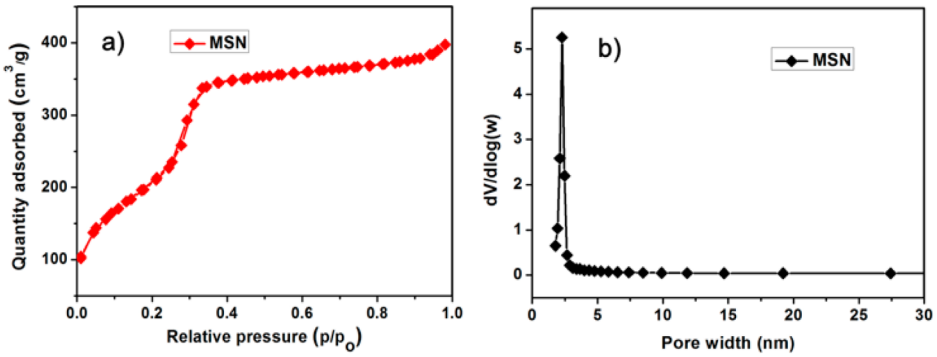

Figure 1. (a) BET isotherm curve of MSN. (b) BJH pore size distribution of MSN.

the high dosage group, the concentrations of AMO and Lys were 0.2 mg mL^{-1} and 0.4 mg mL^{-1}, respectively. While the concentrations of AMO and Lys were 0.06 mg mL^{-1} and 0.12 mg mL^{-1} for the low dosage group. Drugs were applied (0.1 mL) at 4 h after inoculation, twice every day (drug delivery every 12 h). On the third day for postwounding, animals were euthanized by cervical dislocation and the wounds were assessed. Each wounded skin was removed from the animal and then measured for weight, with unwounded skin as the blank control and wounded skin without applying drug taken from the back as the negative control. For each group, tissue samples were removed from the wounds after the rats were sacrificed 4 days upon the treatment for pathology observations. After fixation with 4% phosphate-buffered formaldehyde for at least 24 h, the specimens were embedded in paraffin and sectioned into a thickness of 10 μm. The samples underwent routine histological processing with hematoxylin and eosin. The samples then were observed under a microscope.

RESULTS AND DISCUSSION

Characterization of MSN-Lys-HA-PGMA. According to N_2 adsorption and desorption isotherms (see Figures 1a and 1b), an adsorption step at a P/P_0 value (0.1−0.3) of MSN exhibits characteristic type IV isotherms, confirming the presence of typical mesoscale pores. The specific surface (S_{BET}) value of MSN is 776.54 m^2 g^{-1} based on the Brunauer−Emmett−Teller (BET) model. In addition, a pronounced step is displayed at relative pressures (P/P_0) ranging from 0.2 to 0.7, because of the capillary condensation of nitrogen inside the primary mesoporous material. A narrow Barrett−Joyner−Halenda (BJH) pore size distribution was indicated in accordance with the steep condensation step. As shown in Figure 1b, the pore volumes and pore size of MSN is 0.53 cm^3 g^{-1} and 2.28 nm, respectively.

AMO was loaded into MSN through a reported process.[60] The loading capacity of AMO, which was related to the mesoporous architecture of MSN, was 8.5%. The small molecules like AMO can be easily loaded into the pores of MSN and quickly release when the out layers open. Highest activity could be obtained for Lys at pH values from 5.5 to 6.5.[61] Therefore, Lys was absorbed at pH 6.2 to ensure the highest enzymatic activity.[62] Lys is positively charged with potential value of 23.5 mV and be able to coat onto the negatively charged MSN surface through electrostatic interaction. The assembly process, as well as morphology and size of MSN, MSN-Lys, and MSN-Lys-HA-PGMA were examined by SEM and TEM (Figure 2). MSN samples were spherical in shape bearing a rough surface with an average particle diameter of ~110 ± 10 nm (Figures 2a−c), which is in the same range of a hydrodynamic diameter of 142 ± 21 nm, as observed by DLS (Figure 3a). After AMO loading and coating with Lys, the average particle diameter increased to 132 ± 24 nm (Figure 2d). Finally, the average particle diameter of MSN-Lys-HA and MSN-Lys-HA-PGMA was determined to be 156 ± 15 and 174 ± 26 nm, respectively (Figures 2e and 2f), which agreed with those obtained from DLS. The sizes of the nanoparticles in the adsorption and coating process on MSN were also determined using DLS (Figures 3a−d), which exhibited an increasing size upon LBL absorption, in a good agreement with the observation by microscopy.

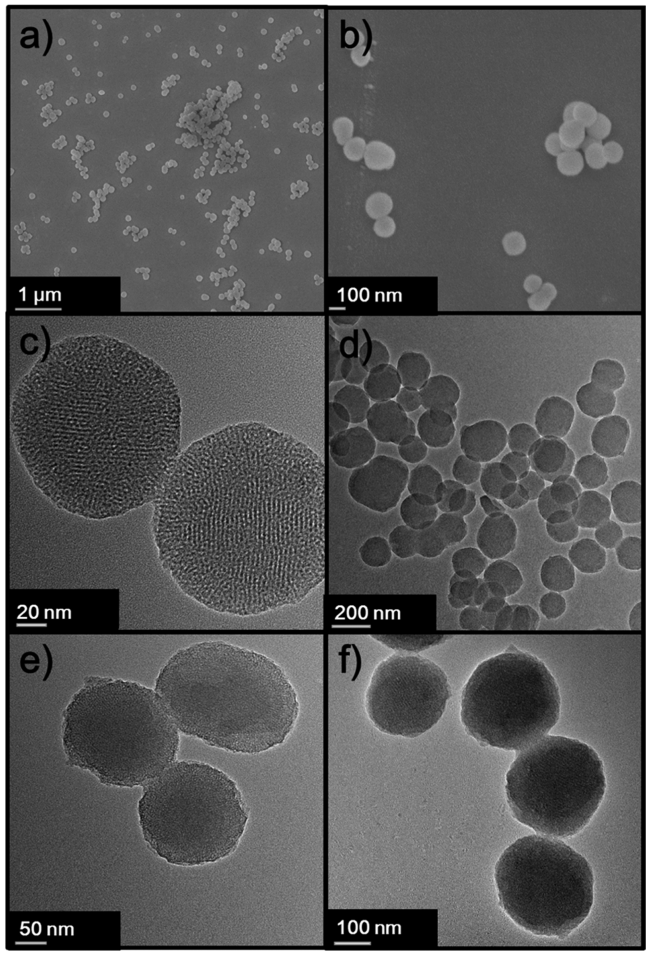

Figure 2. SEM and TEM images of nanoparticles: (a and b) SEM images of MSN; TEM images of (c) MSN, (d) MSN-Lys, (e) MSN-Lys-HA, and (f) MSN-Lys-HA-PGMA.

The hydrodynamic dynamic diameter, with medium polydispersity, increased from 142 nm to 311 nm (Figures 3a−d), which evidenced the coating process. The zeta potential

DOI: 10.1021/acsami.5b04216
ACS Appl. Mater. Interfaces 2015, 7, 17255−17263

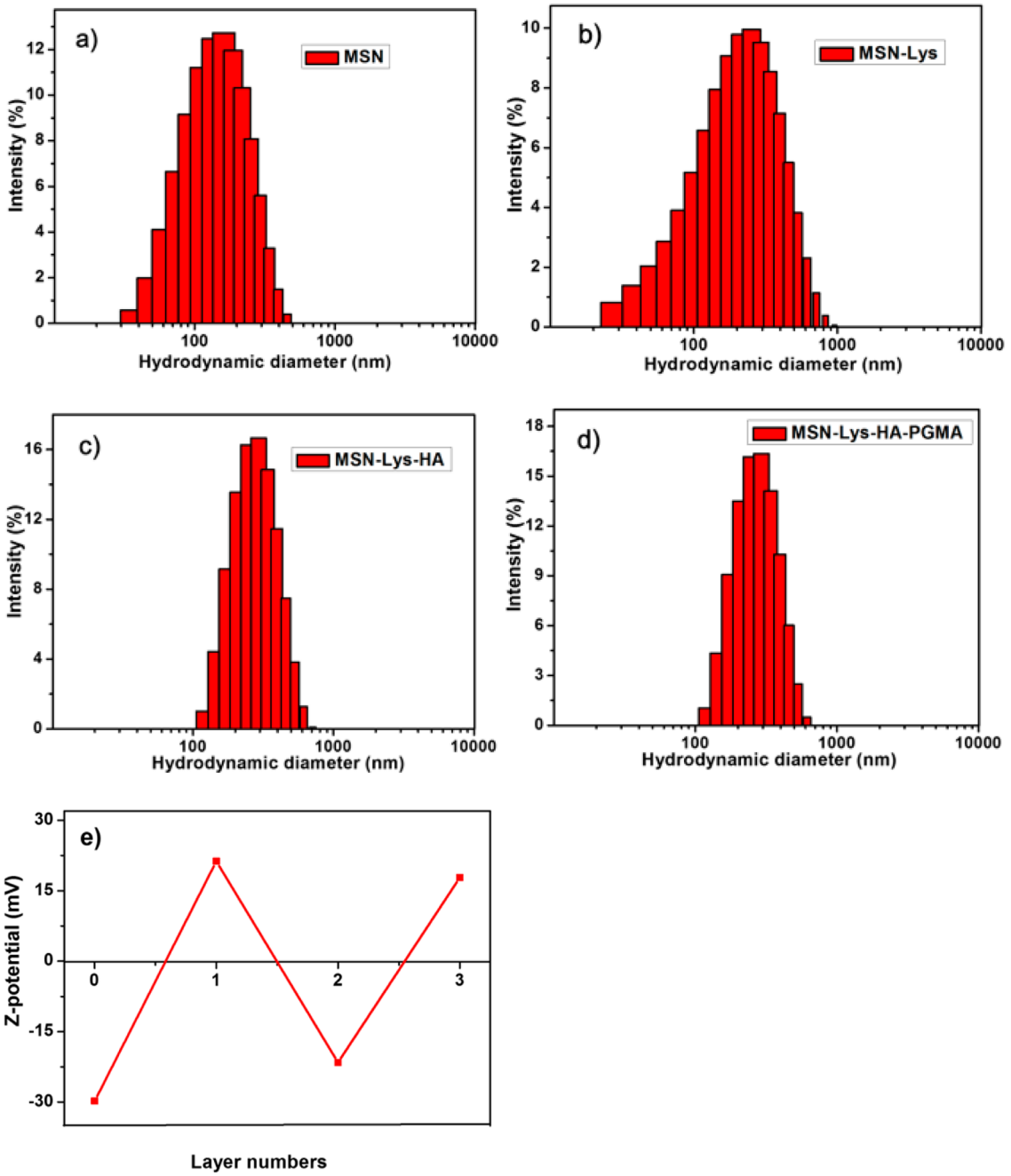

Figure 3. Hydrodynamic diameters and distributions of (a) MSN, (b) MSN-Lys, (c) MSN-Lys-HA, and (d) MSN-Lys-HA-PGMA determined by DLS. (e) Variation of zeta-potentials of MSN-Lys-HA-PGMA during the LBL coating process.

of MSN, MSN-Lys, MSN-Lys-HA and MSN-Lys-HA-PGMA was measured in PBS (Figure 3e). MSN possesses a zeta potential of −29.8 mV, while the zeta potential of MSN-Lys turned to be 21.3 mV upon coating with Lys. The potential turned to be −21.6 mV after further coating with HA. The silica particles with outermost layers of EDA-PGMA showed zeta potentials of 17.8 mV. The alternating zeta potentials observed with each coating step suggest that MSN are successfully coated by electrostatic interactions.

MSN and MSN-Lys-HA-PGMA present well-defined XRD patterns (Figure 4a), where the d_{100} reflections of the hexagonal symmetry can be identified. The aperture of MSN and the change after encapsulation of AMO were detected by XRD. According to Figure 4d, the XRD pattern of pure AMO exhibits complicated characteristic peak while the XRD patterns of MSN showed only one peak. After AMO loading, the characteristic peak of AMO disappeared. Coating of the polyelectrolytes made the diffraction peak broader and weaker (Figure 4b). These results demonstrated that AMO-loaded nanoparticles have been successfully prepared.

Thermogravimetric Analysis (TGA) of MSN-Lys-HA-PGMA. The adsorption amount of polymer and enzyme immobilized on MSN were measured by TGA (Figure 5). We used weight loss to define the adsorption amount of each polyelectrolyte, compared with MSN. For MSN, the weight loss between 25 °C and 1000 °C was ∼16% (Figure 5a), corresponding to the decomposition of carboxyl groups of MSN. The weight loss increased to 28% for AMO-loaded

DOI: 10.1021/acsami.5b04216
ACS Appl. Mater. Interfaces 2015, 7, 17255−17263

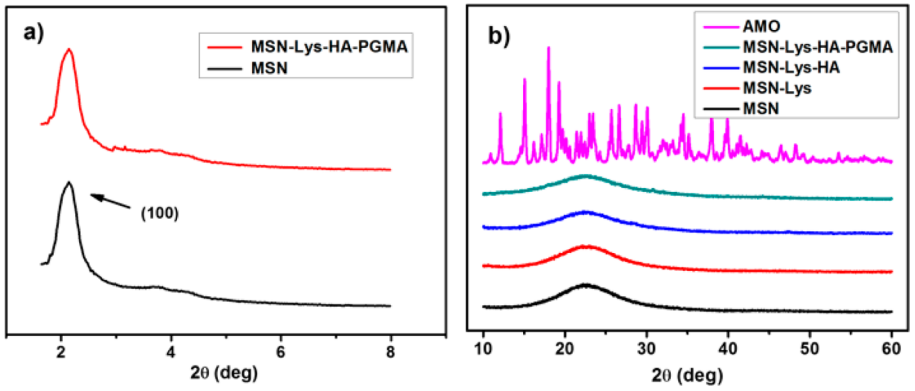

Figure 4. (a) Small-angle XRD of MSN and MSN-Lys-HA-PGMA. (b) XRD of AMO, MSN, MSN-Lys, MSN-Lys-HA, and MSN-Lys-HA-PGMA.

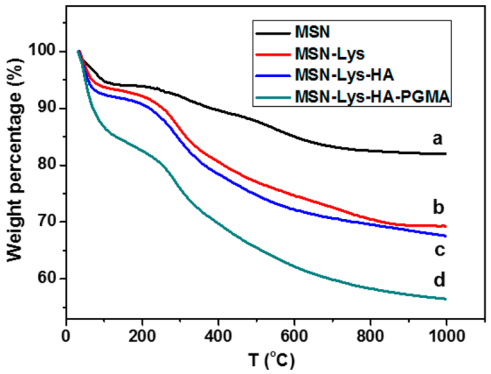

Figure 5. TGA curves recorded for MSN (spectrum a), MSN-Lys (spectrum b), MSN-Lys-HA (spectrum c), and MSN-Lys-HA-PGMA (spectrum d).

MSN-Lys, indicating that the weight percentage of AMO and Lys was ~12% (Figure 5b). After coating with HA and PGMA, the weight loss percentage increased to 34% and 45%, respectively, indicating that the weight percentage of HA and PGMA was 6% and 11%, respectively (Figures 5c and 5d).

Triggered Release of AMO. The enzyme-triggered release of AMO and the split of MSN-Lys-HA-PGMA nanoparticles were investigated by recording the UV absorbance of AMO at 385 nm. The release of loaded AMO could be accelerated with the addition of hyaluronidase, compared with the control without the enzyme (Figure 6). The enzyme hyaluronidase is able to degrade HA. The hyaluronidase, secreted by Gram-positive bacteria (*S. aureus*), leads to the specific cleavage of

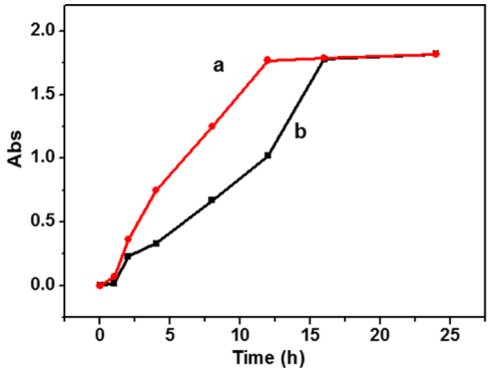

Figure 6. AMO release from MSN-Lys-HA-PGMA in the presence (curve a) and absence (curve b) of hyaluronidase.

MSN-Lys-HA-PGMA, followed by the release of Lys and AMO.

Cytotoxicity and Hemolysis of MSN-Lys-HA-PGMA. Nowadays, the biocompatibility of antimicrobial agents is their major concern for wide application, especially the hemolysis of red blood cells and cytotoxicity to normal cells. To solve these problems, the cell cytotoxicity of MSN-Lys-HA-PGMA to fibroblasts L929 was tested by commercial available CCK-8 assay. The blank carriers showed good biocompatibility, the viabilities were dependent mainly on the nature of its functional groups, because of the nontoxicity of MSN.[63,64] The same trend appeared for the AMO-loaded nanoparticles. No cytotoxicity of MSN-Lys-HA-PGMA was observed to fibroblasts L929 cells, even when the concentration increased to 500 μg mL^{-1} (see Figure 7). Therefore, the LBL formulation exhibited improved cell viability against fibroblasts L929. This result indicated that MSN-Lys-HA-PGMA is safe for normal cells.

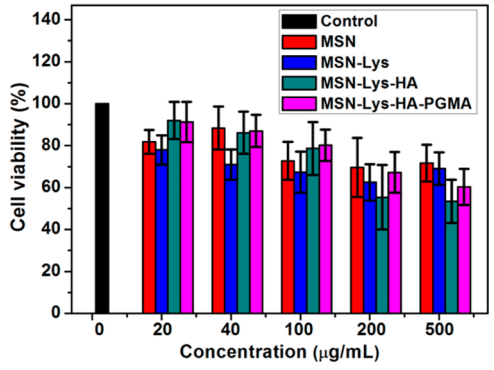

Figure 7. Cell viability assay of Fibroblasts L929 treated with MSN, MSN-Lys, MSN-Lys-HA, and MSN-Lys-HA-PGMA (0–500 μg mL^{-1}).

In addition, the hemolysis of human blood was evaluated by incubation with different concentrations of MSN-Lys-HA-PGMA (2–1000 μg mL^{-1}, 20 μL) with RBC stock. As shown in Figure 8, we did not observe significant hemolytic activity of MSN-Lys-HA-PGMA, even at a concentration up to 1 mg mL^{-1}. The positively charged structures of antibacterial agents, e.g., cationic polymers and antimicrobial peptides, could interact with the negatively surface of charged bacterial cell, and bind with mammalian cell membrane constituents. Therefore, we used EDA-PGMA as the outmost layer to facilitate the cell uptake. This nonspecific recognition mechanism may cause the cytotoxicity and hemolytic activity

DOI: 10.1021/acsami.5b04216
ACS Appl. Mater. Interfaces 2015, 7, 17255–17263

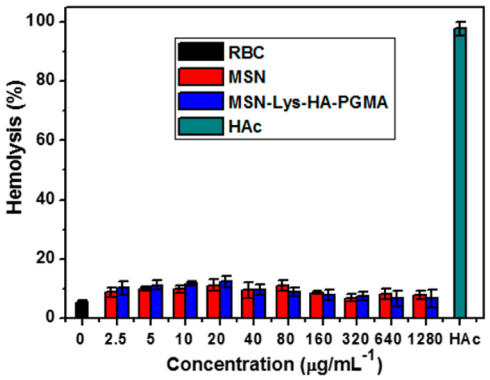

Figure 8. Hemolytic activity of MSN and MSN-Lys-HA-PGMA (2–1000 μg mL^{-1}) with erythrocyte stock in Tris buffer solution. RBCs were used as a negative control and HAc as a positive control.

of traditional antimicrobial agents. However, in this study, MSN-Lys-HA-PGMA was coated with Lys, which was capable of specifically binding to the peptidoglycans on the surface of bacterial cell membrane, showing strong interaction toward the bacteria and negligible hemolytic activity and lower cytotoxicity.

Antibacterial Activity of MSN-Lys-HA-PGMA *In Vitro*. The antibacterial activity of MSN-Lys-HA-PGMA was measured by growth inhibition of AMO-resistant *E. coli* and *S. aureus* with varied concentrations of the nanoparticles. Their optical density after 16 h of incubation was determined at 600 nm ($OD_{600\ nm}$). To confirm the synergistic effects of MSN, Lys, HA, and PGMA-EDA, we tested the zone of inhibition and measured the MIC.

Generally, the more effective antimicrobial materials in the disk will give larger diameters of the clear zone surrounding the disk. According to Figure 9, the diameters of the zones of MSN-Lys-HA-PGMA were significantly larger than those of AMO and Lys alone. Especially, AMO shows almost no inhibition to AMO-resistant bacteria. Apparently, MSN-Lys-HA-PGMA showed excellent antibacterial effects against both

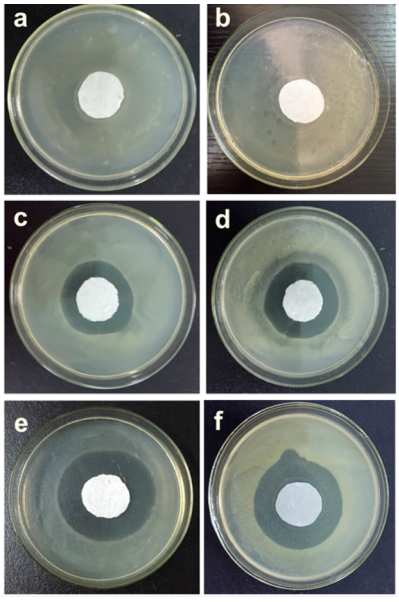

Figure 9. Inhibition zones of (a) AMO, (c) AMO and Lys, and (e) MSN-Lys-HA-PGMA against *E. coli* and (b) AMO, (d) AMO and Lys, and (f) MSN-Lys-HA-PGMA against *S. aureus*.

Gram-negative and Gram-positive bacteria, because of their polyvalent antibacterial effects.

The viability of bacteria was investigated to identify the antibacterial activity of MSN-Lys-HA-PGMA. Bacterial cells with a compromised membrane stain red from EB and viable bacterial cells stain green with AO, which can be observed by the fluorescence microscope. Fluorescence micrographs of *S. aureus* before and after treatment with MSN-Lys-HA-PGMA for 15 min are shown in Figure 10. The untreated bacterial cells

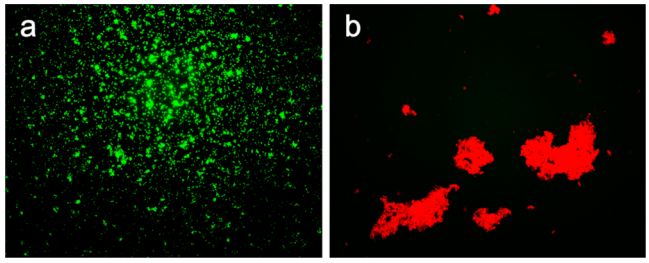

Figure 10. Fluorescence micrograph of (a) *S. aureus* and (b) *S. aureus* after being treated with MSN-Lys-HA-PGMA for 15 min.

were alive with green fluorescence. After treatment with MSN-Lys-HA-PGMA for 15 min, the cells ehibited red fluorescence, indicating they were dead (Figure 10b). Thus, the results suggested that the MSN-Lys-HA-PGMA was able to quickly and efficiently kill the bacteria.

We then explored the antibacterial activity of the composite nanocapsules quantitatively. MSN-Lys showed good antibacterial capacity compared with isodose Lys and AMO. Besides, no obvious *E. coli* or *S. aureus* inhibition effect could be observed even at a concentration of MSN up to 500 μg mL^{-1}. After coating the nanoparticle with HA and EDA-PGMA, much better antibacterial effects emerged. The cationic polymer can interact with bacteria and be implemented on MSN as protective coatings, leading to sustained inhibitory effects. HA can be cleaved when the nanoparticles come across the bacteria because bacteria can produce hyaluronidase. Then, Lys and AMO can bind to bacteria efficiently and quickly damage the cell membrane of bacteria. As shown in Figure 11, the antibacterial efficiency of MSN-Lys-HA-PGMA is much better than isodose AMO and Lys toward AMO-resistant *E. coli* and *S. aureus*. According to the plate count method,[65] the MIC values of MSN-Lys-HA-PGMA toward AMO-resistant *E. coli* and *S. aureus* were, respectively, 62 μg mL^{-1} and 47 μg mL^{-1}, which was much lower than that of free Lys with an MIC of 500 μg mL^{-1}. Because of the protection of the lipopolysaccharide layer surrounding their outmost membrane, Lys exhibits a relatively weak antimicrobial activity for Gram-negative bacillus. Therefore, the inhibition effect of MSN-Lys-HA-PGMA toward *S. aureus* is better than that of *E. coli*.

Antibacterial Activity of MSN-Lys-HA-PGMA *In Vivo*. Complicated skin infections are often caused by Gram-positive bacteria such as *S. aureus*.[66] AMO was widely used in clinical applications against infections. Lys exhibited the best overall synergistic activity with AMO against Gram-positive bacteria *in vitro*, that is, combining Lys with AMO produced potent synergistic effects. Thus, MSN-Lys-HA-PGMA was used to evaluate the antimicrobial effects, *in vivo*, of a mouse wound model infected with *S. aureus*.

The dose of Lys and AMO reduced the amount of bacteria in all of the treatment groups. Table 1 shows that the average

DOI: 10.1021/acsami.5b04216
ACS Appl. Mater. Interfaces 2015, 7, 17255–17263

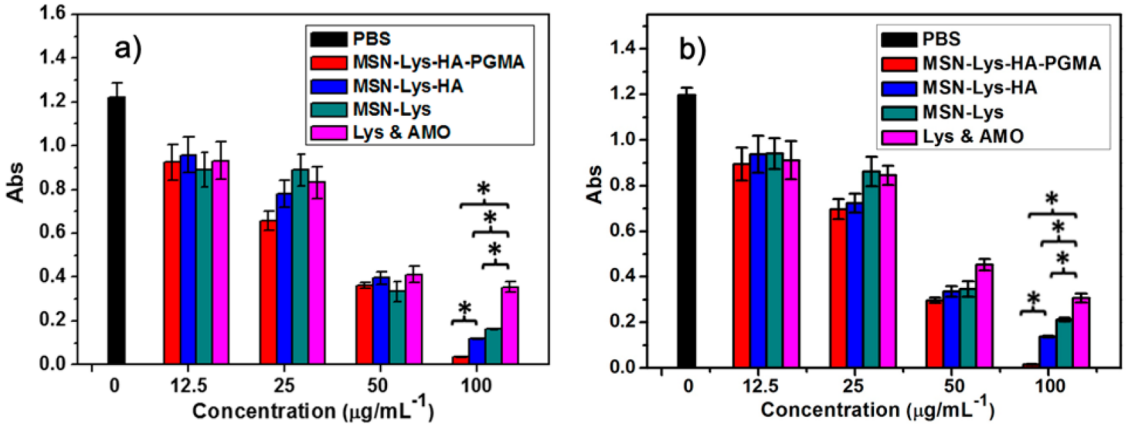

Figure 11. Antibacterial activity of MSN-Lys, MSN-Lys-HA, and MSN-Lys-HA-PGMA toward (a) *E. coli* and (b) *S. aureus*. PBS were chosen as a negative control and the combination of isodose Lys and AMO was chosen as a positive control.

Table 1. Quantitative Culture of Excised Tissues in *S. aureus*

	CFU/mL (average)	bacteriostatic rate (%)
uninfected	$<10^4$	
infected untreated	1.86×10^7	
AMO and Lys (0.1 mg mL^{-1} and 0.2 mg mL^{-1})	3.59×10^6	81.7
MSN-Lys-HA-PGMA	2.36×10^4	99.9

number of bacteria in the untreated controls was remarkably higher than the average number of bacteria in the treatment groups. Epidermal drug delivery with a single dose of Lys and AMO significantly reduced the number of bacteria to a bacteriostatic rate of 67.4%, compared to the negative controls, while the synergistic application of MSN-Lys-HA-PGMA inhibited the most bacteria, with a bacteriostatic rate of 99.9%.

Combination application of the antibiotics and MSN-Lys-HA-PGMA produced synergistic effects due to a dual mode of action against the cell membranes and the cytoplasmic targets. Specifically, the combination of MSN-Lys-HA-PGMA was an effective method that could be used against antibiotic-resistant pathogens. The synergistic effects that were revealed *in vitro* and *in vivo* can lead to a rapid increase in antibacterial activities and delay the emergence of resistance.

To evaluate the state of healing of infected wounds after administration of MSN-Lys-HA-PGMA, we carried out the histological evaluation of rat epidermal wounds on day 7 after treatment. Representative hematoxylin and eosin (H&E)-stained histological images are shown in Figure 12. As compared with the blank control group (Figure 12a) and AMO-Lys group (Figure 12c), the treatment group (Figure 12b) clearly showed the epithelialization, as well as formation of granulation tissue, suggesting antibacterial activities and wound healing. In contrast, we could observe a large number of inflammatory cells and bacteria in the untreated wounds (Figure 12d). These results indicated that MSN-Lys-HA-PGMA had good inhibition for pathogens in bacteria-infected wounds.

CONCLUSION

In conclusion, we presented a biohybrid nanoparticle including antibiotics, enzyme, polymer, hyaluronic acid (HA), and mesoporous silica nanoparticles (MSN), which exhibited effective *in vitro* and *in vivo* antibacterial activity with good

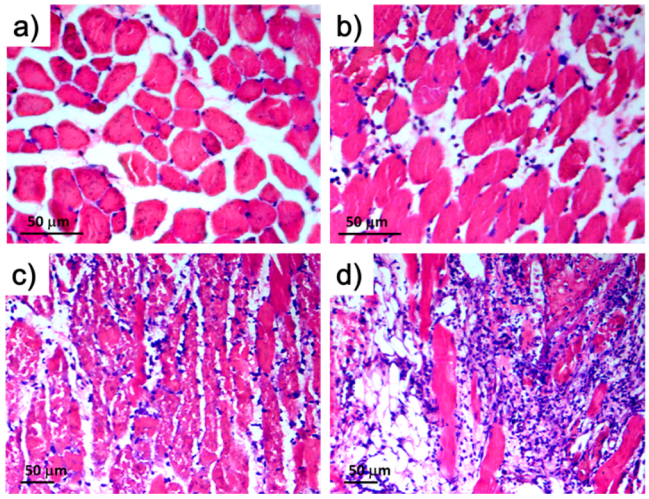

Figure 12. Study on the effects of *S. aureus*-induced wound infections for 3 days ($n = 7$) *in vivo*: (a) normal group, (b) MSN-Lys-HA-PGMA group, (c) AMO and Lys group, and (d) blank control group.

biocompatibility and low hemolytic side effect. The Lys and cationic PGMA derivative of MSN-Lys-HA-PGMA was able to efficiently bind onto the cell membrane of bacteria due to the multivalent interaction. HA worked as an enzyme hyaluronidase-responsive valve for antibacterial release in our system. AMO, Lys, HA, and EDA-PGMA showed a strong synergistic effect and efficient antibacterial ability to drug-resistant bacteria, compared with conventional antibiotics *in vitro*. In addition, *in vivo* experimental results indicated that MSN-Lys-HA-PGMA had good inhibition for pathogens in bacteria-infected wounds. The good biocompatibility and efficient enzyme-responsive drug release ability of the present LBL-coated MSN biohybrid nanomaterials based on Lys, HA, and EDA-PGOHMAs open up an alternative new avenue for the replacement of antibiotics.

ASSOCIATED CONTENT

Supporting Information

Some experimental section including BET analysis, DLS, Lys adsorption isotherms and desorption procedure, TGA, XRD, cytotoxicity assay, hemolysis assay, determination of minimum inhibitory concentration, zone of inhibition test, fluorescence microscopic observations, as well as the results of adsorption and desorption of Lys and circular dichroism. The Supporting

DOI: 10.1021/acsami.5b04216
ACS Appl. Mater. Interfaces 2015, 7, 17255−17263

Information is available free of charge on the ACS Publications website at DOI: 10.1021/acsami.5b04216.

AUTHOR INFORMATION

Corresponding Authors

*E-mail: ywyang@jlu.edu.cn (Y.-W. Yang).
*Tel.: (+86) 2260214259. E-mails: ghhigher@hotmail.com, hgao@tjut.edu.cn (H. Gao).

Notes

The authors declare no competing financial interest.

ACKNOWLEDGMENTS

The authors thank National Natural Science Foundation of China (Nos. 21374079, 21244004, and 51473061), Program for New Century Excellent Talents in University (No. NCET-11-1063), and Program for Prominent Young College Teachers of Tianjin Educational Committee for financial support.

REFERENCES

(1) Travis, J. Reviving the Antibiotic Miracle? *Science* **1994**, *264*, 360−362.
(2) Cohen, M. Epidemiology of Drug Resistance: Implications for a Postantimicrobial Era. *Science* **1992**, *257*, 1050−1055.
(3) Neu, H. C. The Crisis in Antibiotic Resistance. *Science* **1992**, *257*, 1064−1073.
(4) Levy, S. B.; Marshall, B. Antibacterial Resistance Worldwide: Causes, Challenges and Responses. *Nat. Med.* **2004**, *10*, S122−S129.
(5) Lu, X.; Gao, H.; Li, C.; Yang, Y.-W.; Wang, Y. N.; Fan, Y.; Wu, G.; Ma, J. Polyelectrolyte Complex Nanoparticles of Amino Poly(glycerol methacrylate)s and Insulin. *Int. J. Pharm.* **2012**, *423*, 195−201.
(6) Gao, H.; Lu, X.; Ma, Y.; Yang, Y.-W.; Li, J.; Wu, G.; Wang, Y.; Fan, Y.; Ma, J. Amino Poly(glycerol methacrylate)s for Oligonucleic Acid Delivery with Enhanced Transfection Efficiency and Low Cytotoxicity. *Soft Matter* **2011**, *7*, 9239−9247.
(7) Liang, Z.; Wu, X.; Yang, Y.-W.; Li, C.; Wu, G.; Gao, H. Quaternized Amino Poly(glycerol-methacrylate)s for Enhanced pDNA Delivery. *Polym. Chem.* **2013**, *4*, 3514−3523.
(8) Li, C.; Yang, Y.-W.; Liang, Z.; Wu, G.; Gao, H. Post-Modification of Poly(glycidyl methacrylate)s with Alkyl Amine and Isothiocyanate for Effective pDNA Delivery. *Polym. Chem.* **2013**, *4*, 4366−4374.
(9) Latała, A.; Stepnowski, P.; Nedzi, M.; Mrozik, W. Marine Toxicity Assessment of Imidazolium Ionic Liquids: Acute Effects on the Baltic Algae *Oocystis submarina* and *Cyclotella meneghiniana*. *Aquat. Toxicol.* **2005**, *73*, 91−98.
(10) Kido, Y.; Hiramoto, S.; Murao, M.; Horio, Y.; Miyazaki, T.; Kodama, T.; Nakabou, Y. ε-Polylysine Inhibits Pancreatic Lipase Activity and Suppresses Postprandial Hypertriacylglyceridemia in Rats. *J. Nutr.* **2003**, *133*, 1887−1891.
(11) Gilbert, P.; Moore, L. E. Cationic Antiseptics: Diversity of Action under a Common Epithet. *J. Appl. Microbiol.* **2005**, *99*, 703−715.
(12) Ioannou, C.; Hanlon, G.; Denyer, S. Action of Disinfectant Quaternary Ammonium Compounds against *Staphylococcus aureus*. *Antimicrob. Agents Chemother.* **2007**, *51*, 296−306.
(13) Soykan, C.; Coskun, R.; Delibas, A. Microbial Screening of Copolymers of *N*-Vinylimidazole with Phenacyl Methacrylate: Synthesis and Monomer Reactivity Ratios. *J. Macromol. Sci., Part A: Pure Appl.Chem.* **2005**, *42*, 1603−1619.
(14) Lin, J.; Qiu, S.; Lewis, K.; Klibanov, A. Mechanism of Bactericidal and Fungicidal Activities of Textiles Covalently Modified with Alkylated Polyethylenimine. *Biotechnol. Bioeng.* **2003**, *83*, 168−172.
(15) Luo, L.; Li, G.; Luan, D.; Yuan, Q.; Wei, Y.; Wang, X. Antibacterial Adhesion of Borneol-Based Polymer via Surface Chiral Stereochemistry. *ACS Appl. Mater. Interfaces* **2014**, *6*, 19371−19377.
(16) Zhao, J.; Song, L.; Shi, Q.; Luan, S.; Yin, J. Antibacterial and Hemocompatibility Switchable Polypropylene Nonwoven Fabric Membrane Surface. *ACS Appl. Mater. Interfaces* **2013**, *5*, 5260−5268.
(17) Sileika, T.; Kim, H.; Maniak, P.; Messersmith, P. Antibacterial Performance of Polydopamine-Modified Polymer Surfaces Containing Passive and Active Components. *ACS Appl. Mater. Interfaces* **2011**, *3*, 4602−4610.
(18) Li, L.; Wang, H. Enzyme-Coated Mesoporous Silica Nanoparticles as Efficient Antibacterial Agents *In Vivo*. *Adv. Healthcare Mater.* **2013**, *2*, 1351−1360.
(19) Liu, L.; Xu, K.; Wang, H.; Tan, P. K.; Fan, W.; Venkatraman, S.; Li, L.; Yang, Y. Self-assembled Cationic Peptide Nanoparticles as an Efficient Antimicrobial Agent. *Nat. Nanotechnol.* **2009**, *4*, 457−463.
(20) Zetterberg, M.; Reijmar, K.; Pränting, M.; Engström, Å.; Andersson, D.; Edwards, K. PEG-stabilized Lipid Disks as Carriers for Amphiphilic Antimicrobial Peptides. *J. Controlled Release* **2011**, *156*, 323−328.
(21) Hancock, R.; Sahl, H. Antimicrobial and Host-Defense Peptides as New Anti-Infective Therapeutic Strategies. *Nat. Biotechnol.* **2006**, *24*, 1551−1557.
(22) Zasloff, M. Antimicrobial Peptides of Multicellular Organisms. *Nature* **2002**, *415*, 389−395.
(23) Xiu, Z.; Zhang, Q.; Puppala, H.; Colvin, V.; Alvarez, P. Negligible Particle-Specific Antibacterial Activity of Silver Nanoparticles. *Nano Lett.* **2012**, *12*, 4271−4275.
(24) Zhao, Y.; Tian, Y.; Cui, Y.; Liu, W.; Ma, W.; Jiang, X. Small Molecule-Capped Gold Nanoparticles as Potent Antibacterial Agents That Target Gram-Negative Bacteria. *J. Am. Chem. Soc.* **2010**, *132*, 12349−12356.
(25) Jia, Q.; Shan, S.; Jiang, L.; Wang, Y.; Li, D. Synergistic Antimicrobial Effects of Polyaniline Combined with Silver Nanoparticles. *J. Appl. Polym. Sci.* **2012**, *125*, 3560−3566.
(26) Liong, M.; France, B.; Bradley, K.; Zink, J. Antimicrobial Activity of Silver Nanocrystals Encapsulated in Mesoporous Silica Nanoparticles. *Adv. Mater.* **2009**, *21*, 1684−1689.
(27) Ilker, M.; Nüsslein, K.; Tew, G.; Coughlin, E. Tuning the Hemolytic and Antibacterial Activities of Amphiphilic Polynorbornene Derivatives. *J. Am. Chem. Soc.* **2004**, *126*, 15870−15875.
(28) Kenawy, E.; Worley, S.; Broughton, R. The Chemistry and Applications of Antimicrobial Polymers: A State-of-the-Art Review. *Biomacromolecules* **2007**, *8*, 1359−1384.
(29) Murata, H.; Koepsel, R. R.; Matyjaszewski, K.; Russell, A. J. Permanent, Non-leaching Antibacterial Surfaces-2: How High Density Cationic Surfaces Kill Bacterial Cells. *Biomaterials* **2007**, *28*, 4870−4879.
(30) Cado, G.; Aslam, R.; Séon, L.; Garnier, T.; Fabre, R.; Parat, A.; Chassepot, A.; Voegel, J. C.; Senger, B.; Schneider, F.; Frère, Y.; Jierry, L.; Schaaf, P.; Kerdjoudj, H.; Metz-Boutigue, M. H.; Boulmedais, F. Self-Defensive Biomaterial Coating Against Bacteria and Yeasts: Polysaccharide Multilayer Film with Embedded Antimicrobial Peptide. *Adv. Funct. Mater.* **2013**, *23*, 4801−4809.
(31) Li, Y.; Fukushima, K.; Coady, D. J.; Engler, A. C.; Liu, S.; Huang, Y.; Cho, J. S.; Guo, Y.; Miller, L. S.; Tan, P. K.; Ee, P.; Fan, W.; Yang, Y.; Hedrick, J. L. Broad-Spectrum Antimicrobial and Biofilm-Disrupting Hydrogels: Stereocomplex-Driven Supramolecular AsseHmblies. *Angew. Chem., Int. Ed.* **2013**, *52*, 674−678.
(32) Mine, Y.; Ma, F.; Lauriau, S. Antimicrobial Peptides Released by Enzymatic Hydrolysis of Hen Egg White Lysozyme. *J. Agric. Food Chem.* **2004**, *52*, 1088−1094.
(33) Eby, D. M.; Luckarift, H. R.; Johnson, G. R. Hybrid Antimicrobial Enzyme and Silver Nanoparticle Coatings for Medical Instruments. *ACS Appl. Mater. Interfaces* **2009**, *1*, 1553−1560.
(34) Pirnazar, P.; Wolinsky, L.; Nachnani, S.; Haake, S.; Pilloni, A.; Bernard, G. W. Bacteriostatic Effects of Hyaluronic Acid. *J. Periodontol.* **1999**, *70*, 370−374.
(35) Ardizzoni, A.; Neglia, R. G.; Baschieri, M. C.; Cermelli, C.; Caratozzolo, M.; Righi, E.; Palmieri, B.; Blasi, E. Influence of Hyaluronic Acid on Bacterial and Fungal Species, Including Clinically

Relevant Opportunistic Pathogens. *J. Mater. Sci.: Mater. Med.* **2011**, *22*, 2329−2338.
(36) Ouasti, S.; Kingham, P. J.; Terenghi, G.; Tirelli, N. The CD44/integrins Interplay and the Significance of Receptor Binding and Representation in the Uptake of RGD-Functionalized Hyaluronic Acid. *Biomaterials* **2012**, *33*, 1120−1134.
(37) Vazquez, J. R.; Short, B.; Findlow, A. H.; Nixon, B. P.; Boulton, A. J. M.; Armstrong, D. G. Diabetes Outcomes of Hyaluronan Therapy in Diabetic Foot Wounds. *Diabetes Res. Clin. Pract.* **2003**, *59*, 123−127.
(38) Gao, F.; Yang, C. X.; Mo, W.; Liu, Y. W.; He, Y. Q. Hyaluronan Oligosaccharides are Potential Stimulators to Angiogenesis via RHAMM Mediated Signal Pathway in Wound Healing. *Clin. Invest. Med.* **2008**, *31*, 106−116.
(39) Campo, G. M.; Avenoso, A.; Campo, S.; D'Ascola, A.; Nastasi, G.; Calatroni, A. Small Hyaluronan Oligosaccharides Induce Inflammation by Engaging Both Toll-like-4 and CD44 Receptors in Human Chondrocytes. *Biochem. Pharmacol.* **2010**, *80*, 480−490.
(40) Habibi, N.; Pastorino, L.; Soumetz, F. C.; Sbrana, F.; Raiteri, R.; Ruggiero, C. Nanoengineered Polymeric S-Layers Based Capsules with Targeting Activity. *Colloids Surf., B* **2011**, *88*, 366−372.
(41) Hart, M. E.; Hart, J. M.; Roop, A. Genotypic and Phenotypic Assessment of Hyaluronidase among Type Strains of a Select Group of Staphylococcal Species. *Int. J. Microbiol.* **2009**, *2009*, 614371.
(42) Stern, R.; Kogan, G.; Jedrzejas, M. J.; Soltes, L. Biotechnol. The Many Ways to Cleave Hyaluronan. *Biotechnol. Adv.* **2007**, *25*, 537−557.
(43) Sun, Y.-L.; Yang, B.-J.; Zhang, S. X.-A.; Yang, Y.-W. Cucurbit[7]uril Pseudorotaxane-Based Photo-Responsive Supramolecular Nanovalve. *Chem.—Eur. J.* **2012**, *18*, 9212−9216.
(44) Sun, Y.-L.; Yang, Y.-W.; Chen, D.-X.; Wang, G.; Zhou, Y.; Wang, C.-Y.; Stoddart, J. F. Mechanized Silica Nanoparticles Based on Pillar[5]arenes for On-Command Cargo Release. *Small* **2013**, *9*, 3224−3229.
(45) Angelos, S.; Yang, Y.-W.; Patel, K.; Stoddart, J. F.; Zink, J. I. pH-Responsive Supramolecular Nanovalves Based on Cucurbit[6]uril Pseudorotaxanes. *Angew. Chem., Int. Ed.* **2008**, *47*, 2222−2226.
(46) Lin, Y. S.; Haynes, C. L. Impacts of Mesoporous Silica Nanoparticle Size, Pore Ordering, and Pore Integrity on Hemolytic Activity. *J. Am. Chem. Soc.* **2010**, *132*, 4834−4842.
(47) Vallet-Regí, M.; Balas, F.; Arcos, D. Mesoporous Materials for Drug Delivery. *Angew. Chem., Int. Ed.* **2007**, *46*, 7548−7558.
(48) Akcakayiran, D.; Mauder, D.; Hess, C.; Sievers, T. K.; Kurth, D. G.; Shenderovich, I.; Limbach, H. H.; Findenegg, G. H. Carboxylic Acid-Doped SBA-15 Silica as a Host for Metallo-supramolecular Coordination Polymers. *J. Phys. Chem. B* **2008**, *112*, 14637−14647.
(49) Lai, C.-Y.; Trewyn, B. G.; Jeftinija, D. M.; Jeftinija, K.; Xu, S.; Jeftinija, S.; Lin, S. Y. Mesoporous Silica Nanosphere-Based Carrier System with Chemically Removable CdS Nanoparticle Caps for Stimuli-Responsive Controlled Release of Neurotransmitters and Drug Molecules. *J. Am. Chem. Soc.* **2003**, *125*, 4451−4459.
(50) Vivero-Escoto, J. L.; Slowing, I. I.; Wu, C.; Lin, S. Y. Photoinduced Intracellular Controlled Release Drug Delivery in Human Cells by Gold-Capped Mesoporous Silica Nanosphere. *J. Am. Chem. Soc.* **2009**, *131*, 3462−3463.
(51) Liu, R.; Zhang, Y.; Zhao, X.; Agarwal, A.; Mueller, L. J.; Feng, P. pH-Responsive Nanogated Ensemble Based on Gold-Capped Mesoporous Silica through an Acid-Labile Acetal Linker. *J. Am. Chem. Soc.* **2010**, *132*, 1500−1501.
(52) Zhu, C.; Lu, C.; Song, X.; Yang, H.; Wang, X. Bioresponsive Controlled Release Using Mesoporous Silica Nanoparticles Capped with Aptamer-Based Molecular Gate. *J. Am. Chem. Soc.* **2011**, *133*, 1278−1281.
(53) Bernardos, A.; Aznar, E.; Marcos, M. D.; Martínez-Máñez, R.; Sancenón, F.; Soto, J.; Barat, J. M.; Amoros, P. Enzyme-Responsive Controlled Release Using Mesoporous Silica Supports Capped with Lactose. *Angew. Chem.* **2009**, *121*, 5998−6001.
(54) Singh, N.; Karambelkar, A.; Gu, L.; Lin, K.; Miller, J. S.; Chen, C. S.; Sailor, M. J.; Bhatia, S. N. Bioresponsive Mesoporous Silica Nanoparticles for Triggered Drug Release. *J. Am. Chem. Soc.* **2011**, *133*, 19582−19585.
(55) Li, Q.-L.; Wang, L.-Z.; Qiu, X.-L.; Sun, Y.-L.; Wang, P.-X.; Liu, Y.; Li, F.; Qi, A.-D.; Gao, H.; Yang, Y.-W. Stimuli-Responsive Biocompatible Nanovalve Based on β-Cyclodextrin Modified Poly(Glycidyl Methacrylate). *Polym. Chem.* **2014**, *5*, 3389−3395.
(56) Sun, Y.; Sun, Y.-L.; Wang, L.; Ma, J.; Yang, Y.-W.; Gao, H. Nanoassembles Constructed from Mesoporous Silica Nanoparticles and Surface-Coated Multilayer Polyelectrolytes for Controlled Drug Delivery. *Microporous Mesoporous Mater.* **2014**, *185*, 245−253.
(57) Li, Q.-L.; Sun, Y.; Sun, Y.-L.; Wen, J.; Zhou, Y.; Bing, Q.; Isaacs, L.; Jin, Y.; Gao, H.; Yang, Y.-W. Mesoporous Silica Nanoparticles Coated by Layer-by-Layer Self-Assembly Using Cucurbit[7]uril for *In Vitro* and *In Vivo* Anticancer Drug Release. *Chem. Mater.* **2014**, *26*, 6418−6431.
(58) Song, N.; Yang, Y.-W. Molecular and Supramolecular Switches on Mesoporous Silica Nanoparticles. *Chem. Soc. Rev.* **2015**, *44*, 3474−3504.
(59) Yang, Y.-W.; Sun, Y.-L.; Song, N. Switchable Host−Guest Systems on Surfaces. *Acc. Chem. Res.* **2014**, *47*, 1950−1960.
(60) Vallet-Regí, M.; Doadrio, J. C.; Doadrio, A. L.; Izquierdo-Barba, I.; Pérez-Pariente, J. Hexagonal Ordered Mesoporous Material as a Matrix for the Controlled Release of Amoxicillin. *Solid State Ionics* **2004**, *172*, 435−439.
(61) Chipman, D. M.; Sharon, N. Mechanism of Lysozyme Action. *Science* **1969**, *165*, 454−465.
(62) Xue, M. J.; Findenegg, G. H. Lysozyme as a pH-Responsive Valve for the Controlled Release of Guest Molecules from Mesoporous Silica. *Langmuir* **2012**, *28*, 17578−17584.
(63) Hynes, W. L.; Walton, S. L. Hyaluronidases of Gram-Positive Bacteria. *FEMS Microbiol. Lett.* **2000**, *183*, 201−207.
(64) Slowing, I. I.; Trewyn, B. G.; Giri, S.; Lin, V. S. Y. Mesoporous Silica Nanoparticles for Drug Delivery and Biosensing Applications. *Adv. Funct. Mater.* **2007**, *17*, 1225−1236.
(65) Breeuwer, P.; Abee, T. Assessment of Viability of Microorganisms Employing Fluorescence Techniques. *Int. J. Food Microbiol.* **2000**, *55*, 193.
(66) Nichols, R. L.; Graham, D. R.; Barriere, S. L.; Rodgers, A.; Wilson, S. E.; Zervos, M.; Dunn, D. L.; Kreter, B. Treatment of Hospitalized Patients with Complicated Gram-Positive Skin and Skin Structure Infections: Two Randomized, Multicentre Studies of Quinupristin/dalfopristin versus Cefazolin, Oxacillin or Vancomycin. *J. Antimicrob. Chemother.* **1999**, *44*, 263−273.

DOI: 10.1021/acsami.5b04216
ACS Appl. Mater. Interfaces 2015, 7, 17255−17263